

FREQUENCY RATIO OF Al^+ AND Hg^+ SINGLE-ION OPTICAL CLOCKS; METROLOGY AT THE 17TH DECIMAL PLACE

A. Bruschi¹, T. Rosenband¹, D.B. Hume¹, P.O. Schmidt², C.W. Chou¹, L. Lorini³,
W.H. Oskay⁴, R.E. Drullinger¹, T.M. Fortier¹, J.E. Stalnaker⁵, S.A. Diddams¹,
W.C. Swann¹, N.R. Newbury¹, W.M. Itano¹, D.J. Wineland¹, and J.C. Bergquist¹

¹*Time and Frequency Division, National Institute of Standards and Technology, Boulder, CO 80305, USA*

²*Present address: Institut für Experimentalphysik, Universität Innsbruck*

³*Present address: Istituto Nazionale di Ricerca Metrologica (INRiM),
Strada delle Cacce 91, I-10135 Torino, Italy*

⁴*Present address: Stanford Research systems, Sunnyvale, CA, USA*

⁵*Present address: Department of Physics and Astronomy,
Oberlin College, Oberlin, OH 44074, USA*

Optical and microwave atomic clock frequency comparisons at NIST over the past several years provide some of the best tests of any present-day, temporal variations of the fundamental constants. Notably, the increasingly precise measurements of the absolute frequency of the Hg^+ single-ion optical clock and the cesium primary frequency standard NIST-F1, now constrain the fractional variation of the fine structure constant α to less than $2 \cdot 10^{-16} \text{yr}^{-1}$. The measurements of the frequency ratio of the Al^+ and Hg^+ optical clocks, which now reach a fractional frequency uncertainty of $5.2 \cdot 10^{-17}$, offer a 10-fold tighter constraint in just one year. The record of such measurements over the last year sensitively tests and restricts any temporal variation of α to $\dot{\alpha}/\alpha = -1.6 \pm 2.3 \cdot 10^{-17} \text{yr}^{-1}$, consistent with zero.

I. INTRODUCTION

Recently, interest in possible temporal variations of the fundamental "constants" was stirred by conflicting analyses of astrophysical [1] and geophysical data that offer evidence of change [2]. Even a small change of a fundamental constant, either in space or time, would violate one or more tenets of several, widely accepted physical theories. The conflicting claims of temporal change found using different methods, and its important ramifications if true, have triggered a number of experimental efforts toward finding non-ambiguous evidence of any

change [3] [4].

One such approach is to measure the frequency ratios of two or more laboratory atomic clocks over time. The optical clock ratio measurements have now reached an accuracy sufficiently high that a yearlong search for a time variation of α , can be done with a sensitivity comparable to and possibly higher than that offered by the geological and cosmological observations.

The National Institute of Standards and Technologies (NIST) in Boulder, Colorado (USA), hosts several atomic clocks, including optical atomic clock prototypes based on $^{199}\text{Hg}^+$ [5], $^{27}\text{Al}^+$, [6], Ca [7] and Yb [8], as well as the Cs primary frequency standard, NIST-F1 [9] and several commercial Hydrogen Masers. However, in this report we concentrate our discussion on the first results of a direct measurement of the frequency ratio of the Hg^+ and Al^+ optical clocks. We begin with a brief description of the Hg^+ single ion optical frequency standard, which will focus on some technical improvements that were recently introduced, the Al^+ standard, and the techniques for the measurements of their frequency ratio. An error budget for each standard is given as well as the past year's measurements of their frequency ratio. From the results of these frequency comparisons, an estimate of the temporal stability of the constant α will be provided.

II. $^{199}\text{Hg}^+$ FREQUENCY STANDARD

The single Hg^+ ion is confined in a spherical Paul trap that is kept in a cryogenic environment at or near the liquid helium temperature of 4.2 K. The cryogenic temperature provides an ultra high vacuum environment where the collisions with background gases are rare and ion lifetimes of several months have been demonstrated [10]. The trap itself comprises one ring electrode placed between two endcaps. The ring electrode is driven with an oscillating electric field at approximately 12 MHz. At the usual RF operational parameters, the secular frequencies in the radial plane are nearly degenerate with $\omega_x \approx \omega_y \approx (2\pi \cdot 1250 \text{ kHz})$ and the secular frequency along the trap axis $\omega_z \approx (2\pi \cdot 2300 \text{ kHz})$. DC voltages can be applied to the endcaps as well as to two other compensation electrodes, to balance the effect of any stray charges. This makes it possible to minimize the second order Doppler shift and AC Stark shift associated with micromotion at the RF drive frequency.

The $^{199}\text{Hg}^+$ standard uses the $5d^{10}6s \ ^2S_{1/2} \rightarrow 5d^{10}6p \ ^2P_{1/2}$ resonance line at 194 nm for laser cooling, state preparation and detection. The standard as well as the generation of light at 194 nm are described more fully elsewhere [11], [12], [13], [14]. In this section we note only briefly the recent improvements to the system. The first of these is the use of a laser tuned to the $F = 1 \rightarrow F' = 1$ component of the 194 nm transition. The application of this laser rapidly prepares the ion in the $^2S_{1/2}, (F = 0)$ ground state prior to each probe of the clock transition. The new setup has reduced the time required for the state preparation from about 15 ms to 1-2 ms [13]. The second improvement is the use of a laser tuned to resonance with the $^2D_{5/2}(F = 2) \rightarrow ^2P_{3/2}(F = 2)$ transition at 398 nm. This leads to fast depletion of the clock state following the state detection. These improvements lead to a significant reduction of dead time in the clock cycle from about 80 ms to 20 ms, improving the clock duty cycle from 33% to 66% [13], [14].

The clock laser is based on frequency quadrupling a Yb-doped fiber laser, operating at

1126 nm. The IR power of this master laser is amplified to about 600-700 mW with an Yb-doped fiber amplifier and then doubled to 563 nm using a non-critically phase-matched LBO crystal placed in the tight waist of a power enhancement cavity. About 175 mW of green light at 563 nm is generated, most of which is sent through an optical fiber to an acoustically isolated room. The quiet room houses the high-finesse cavity to which the laser is referenced using the Pound-Drever-Hall technique [15]. This system has also been described in detail elsewhere [16]. The stabilized green light is returned to the laboratory through a fiber with noise cancellation. The probe light is then single-passed through a final stepping AOM that is used to step the frequency of the laser back and forth across the ion resonance [17]. The modulated light is doubled to 282 nm in a non-critically phase-matched deuterated AD*P crystal and steered onto the ion. The stepping AOM also serves to cancel the Doppler noise associated with motion of the trap, caused, for example, by the boiling cryogenes.

The clock transition is driven by a single (Rabi) pulse with a typical probe time of 40-60 ms. Following the Rabi pulse, the 194 nm light is turned on for a 5-10 ms detection period. If the detection pulse projects the ion into the $^2S_{1/2}(F = 0)$ state, the 194 nm fluorescence is high (typically 12-15 counts/ms), and no clock transition is recorded. If the clock transition does occur, then the ion remains shelved in the excited $^2D_{5/2}(F = 2)$ clock state and no fluorescence is observed (less than 1 count/ms background) [18]. The Hg^+ clock timing and operations are controlled by software and the clock cycle is looped continuously. The probe light frequency is stepped with a modulation depth equal to the FWHM of the Fourier transform limited linewidth of the probe period. The algorithm for the laser frequency servo uses dedicated algorithms to correct for signal amplitude fluctuation and cavity frequency drift [13].

A. Accuracy of the Hg^+ standard

The various contributions to the systematic fractional frequency uncertainty of the Hg^+ optical clock have been described in detail previously [19]. Since then, the uncertainty due to some contributions have been constrained to lower values. A summary of the contributions to the total systematic fractional frequency uncertainty σ , which is now evaluated to be $\sigma < 1.9 \cdot 10^{-17}$, is reported in detail in table I and summarized in [20], together with the fractional frequency shift $\Delta\nu/\nu$:

The residual motion of the laser-cooled ion gives rise to a fractional frequency uncertainty associated with the relativistic Doppler shift. The uncertainty due to the secular motion is constrained to $4 \cdot 10^{-18}$ when the ion is cooled to near the Doppler cooling limit; the uncertainty due to residual micromotion is also constrained to $4 \cdot 10^{-18}$ when the trap is well balanced. The micromotion of the trap is continuously monitored [21], and, if need be, corrected using small bias voltages applied to either endcap and/or to two bias electrodes that lie exterior to the trap. The bias electrodes are orthogonal to the trap axis and lie 90° apart. The maximum AC Zeeman shift due to any asymmetry of the RF currents flowing in the trap electrodes is now estimated to be $< 1.0 \cdot 10^{-17}$. We believe this latest estimate is more realistic, but remains conservative because it postulates an imbalance of 25% in the rf currents flowing in the trap electrodes [20]. The clock transition is first-order field insensitive at zero field whereas the second-order sensitivity is approximately $-(188 \mu\text{Hz}) \cdot B^2$ (B in μT). The quadratic field shift of the clock transition due to the small ($8 \mu\text{T}$) applied quantization field is effectively monitored during the measurement run by occasionally interleaving a frequency measurement of the first-order field sensitive $^2S_{1/2}(F=0, m_F=2) \rightarrow ^2D_{5/2}(F=2, m_F=2)$ component with the regular clock cycles. Slow variations of the magnetic field presently limit the uncertainty of the DC quadratic Zeeman shift to $5 \cdot 10^{-18}$.

The electronic charge density of the $^2D_{5/2}$ state has an electric quadrupole moment that

can produce an energy shift in the presence of a static electric field gradient. The magnitude and sign of the shift depend on the relative strength of the field gradient and its orientation to the applied field, which offers a route to its cancellation [22]. Typically, the fractional frequency shift of this term is less than 10^{-16} , but due to our inability to know, much less control the ambient field gradient, the uncertainty is equally as large as 10^{-16} [5], [20]. However, the quadrupole shift, as well its uncertainty, can be effectively eliminated by averaging the clock frequency for three mutually perpendicular field quantization axes [22]. In our realization of this scheme, the orientation of the three axes and the probe light polarization were chosen to give the same scattering rate for the clock transition over the three directions of the applied field [19]. Changing the field direction at a regular interval (typically, every 300s) and steering the frequency of the clock laser to resonance with the ion at each field setting are completely automated. The average clock frequency for the three field directions is without the quadrupole shift with a residual uncertainty estimated smaller than 10^{-17} , that is due to the slight non-orthogonality of the three applied fields.

Another potential shift arises from the pulsed interrogation and detection sequence. If the ion is caused to move synchronously with each clock cycle, this would cause a first-order Doppler shift with a non zero average. This synchronized movement could have different sources, for example, the creation of photoionization charges on the trap electrodes due to the scattering of UV light. The systematic shift from this effect is potentially large, as a synchronized velocity of only 10^{-8} m/s due to few photoionization charges, would cause a Doppler shift of $3 \cdot 10^{-17}$ [20]. The effect can be measured and averaged away by alternately probing the ion clock resonance with collinear but counter-propagating beams; no shift was detected at the $7 \cdot 10^{-18}$ level. This value is limited by the unequal statistical weight of probe directions and it can be greatly reduced by averaging equally during the measurement run.

The cryogenic surfaces cryo-pump all gases

TABLE I: Leading contributions to the systematic uncertainty budget of the Hg^+ and Al^+ optical clocks ($\times 10^{-18}$)

Shift	$\Delta\nu_{\text{Hg}}$	σ_{Hg}	$\Delta\nu_{\text{Al}}$	σ_{Al}	Limitation
2^{nd} order Dopp. - Micromotion	-4	4	-20	20	Static electric field
2^{nd} order Dopp. - Secular motion	-3	3	-16	8	Doppler cooling
DC quadratic Zeeman	-1130	5	-453	0.5	B field Cal.
AC quadratic Zeeman	0	10	0	1	Trap RF B-fields
Quadrupole shift	0	10	0	0.5	B-field orientation
1^{st} order Dopp.	0	7	0	1	Probe beam alignment
Background gas	0	4	0	0.5	Collisions rate
AOM phase chirp	0	6	0	0.1	RF power
Blackbody rad.	0	0	-12	5	DC polarizability
Total	-1137	19	-513	23	

with the possible exception of He (which is also cryo-pumped until a monolayer is established). Possible sources of He are leaks in the indium seals as well as through the Dewar windows that are permeable to He. An upper limit to the He partial pressure was set at $7 \cdot 10^{-10}$ Pa using a quadrupole mass analyzer, which is conservatively estimated to give a maximum fractional frequency shift of $4 \cdot 10^{-18}$ [20].

An often overlooked frequency shift is caused by the thermal loading of any AOM in the clock beam path that is turned on and off, such as the stepping AOM used here to probe either side of the clock resonance. The shift scales linearly with RF power, but diminishes with the ratio of time-on to time-off. The typical level of applied power during the probe "on" phase gives a maximum fractional frequency shift of $6 \cdot 10^{-18}$.

III. $^{27}\text{Al}^+$ FREQUENCY STANDARD

As early as 1973, Dehmelt pointed to the group IIIA ions as attractive candidates for optical clocks of high stability and accuracy [18]. In particular, the weakly allowed $^1S_0 \rightarrow ^3P_0$ intercombination line at 267 nm in $^{27}\text{Al}^+$ seemed well suited for building a single-ion optical clock with exceptional stability and accuracy. $^{27}\text{Al}^+$ offer, for example, a 20 s lifetime of the metastable 3P_0 state, no electric quadrupole shift, and a blackbody radiation shift that is

the fractionally of order $-1 \cdot 10^{-17}$ at 50 °C.

Fortunately, the wavelength of the strongly allowed first resonance transition in $^{27}\text{Al}^+$ is at 167 nm, an impractical color for laser cooling and detection. To overcome this limitation, the Al^+ ion is trapped in a linear Paul trap together with a $^9\text{Be}^+$ ion, which has a cycling transition at a convenient wavelength for laser cooling and state manipulation. In this configuration, the motional degrees of freedom of both ions are coupled via the coulomb interaction making it possible to sympathetically cool the $\text{Be}^+ - \text{Al}^+$ ion crystal to the axial ground state by laser-cooling the Be^+ ion [23]. Furthermore, the superposition state of the clock ion can be faithfully transferred to the Be^+ ion through one of their shared motional states using some of the techniques of quantum information processing. This makes it possible to determine the clock state of the Al^+ ion (or of any clock ion) by detecting the state of the Be^+ ion using fluorescence detection[24], [13].

The clock state detection procedure has been described in detail in earlier publications [25] [6], and we only outline the process here. The two relevant energy levels in Be^+ will be labeled $|\downarrow_{\text{Be}}\rangle$ and $|\uparrow_{\text{Be}}\rangle$ corresponding respectively to the $F = 2$ and $F = 1$ hyperfine levels of the $^2S_{1/2}$ ground state. These states can be distinguished with better than 95% fidelity by fluorescence detection through the strong $^2P_{3/2}$ resonance. The relevant electronic states in the

Al⁺ atomic system will be identified by spectroscopic notation as $|^1S_0\rangle$, $|^3P_0\rangle$ and $|^3P_1\rangle$, where the first two are the clock states to be measured and the third is an auxiliary state used as follows: After interrogation of the clock transition and ground state cooling, the ions are in the state $(\alpha|^1S_0\rangle + \beta|^3P_0\rangle)|\downarrow_{Be}\rangle|0\rangle_m$, where $|n\rangle_m$ indicates the n th Fock state of motion. The object of the state mapping procedure is to map the state probabilities $|\alpha|^2$ and $|\beta|^2$ to the Be⁺ electronic states where they can be detected. To do this we first apply a laser pulse tuned to the first motional sideband of the $|^1S_0\rangle \rightarrow |^3P_1\rangle$ resonance. With the appropriate pulse time this produces the state $(\alpha|^3P_1\rangle|1\rangle_m + \beta|^3P_0\rangle|0\rangle_m)|\downarrow_{Be}\rangle$, where the Al⁺ electronic state is now generally entangled with the collective motion. The information stored in the motion can be mapped to the Be⁺ electronic states by use of a laser pulse tuned to the first motional sideband of the qubit transition. This leaves the system in the state $(\alpha|^3P_1\rangle|\uparrow_{Be}\rangle + \beta|^3P_0\rangle|\downarrow_{Be}\rangle)|0\rangle_m$. In this ideal representation of the process, detection of the Be⁺ qubit will replicate statistics for direct detection of Al⁺, however, imperfections in the state mapping limit the fidelity of a single shot to near 85%. This limitation can be circumvented by using the quantum nondemolition nature of the detection interactions to repeat the procedure many times, leading to a fidelity for clock state discrimination as high as 99.94%.

Since every transition between magnetic sublevels of the Al⁺ clock states suffers a first-order linear field shift, which can be as high as few kHz at the operational magnetic field, the stretched magnetic substate's are alternately probed to zero the first-order Zeeman shift. The main contributions to the frequency uncertainty of the standard are listed in table I and is evaluated to $2.3 \cdot 10^{-17}$ [20]. The main contribution to the uncertainty is due to the second-order Doppler shift caused by the residual ion movement related to the secular motion and to the micromotion. Other minor contributions are due to the Zeeman quadratic shift and to the AC Stark shift caused by blackbody radiation at room temperature, which is frac-

tionally of order 10^{-17} , and has been measured in [26]

A. Al⁺/Hg⁺ frequency ratio measurements

The frequency ratio of Al⁺ to Hg⁺ is measured using one and sometimes two different femto second frequency combs (FSFC). The measured light is sent to the FSFC's through noise compensated optical fibers [17]. The first FSFC is based on a Ti:S laser and has been used for all the measurements reported here. In addition, a fiber based FSFC has been used for a significant amount of measurements to produce an independent measurement of the ratio. During the measurements, a single comb line of the FSFC is locked to one of the clocklasers, typically the Hg⁺ laser, while the offset frequency is referenced to the H-maser. This fixes the the frequency of all the lines in the comb, and the beat between one of these lines and the light from the second standard is then counted. The duration of a typical run is several hours. Figure 1a shows the fractional frequency instability of the two optical standards for a typical run using two estimators; the two-sample Allan Deviation and the overlapping sample deviation. For integration times longer than 100 s, when the frequencies of the optical clocks are fully steered by the atoms, the fractional frequency instability is $3.9 \cdot 10^{-15} \tau^{-1/2}$ [20].

Figure 1b shows the frequency ratio measurements of Al⁺ to Hg⁺ from December 2006 to December 2007. The accuracy evaluation for the optical clocks that include first order Doppler shifts synchronized with the probe times has been carried out only for the last four points. The weighted average of the frequency ratio from these measurements, is [20]:

$$f_{Al^+}/f_{Hg^+} = 1.05287183314899044(5) \quad (1)$$

The systematic fractional frequency uncertainties of Hg⁺ ($1.9 \cdot 10^{-17}$) and Al⁺ ($2.3 \cdot 10^{-17}$) contributes nearly equally to the overall fractional frequency uncertainty of the ratio. The fractional frequency uncertainty of

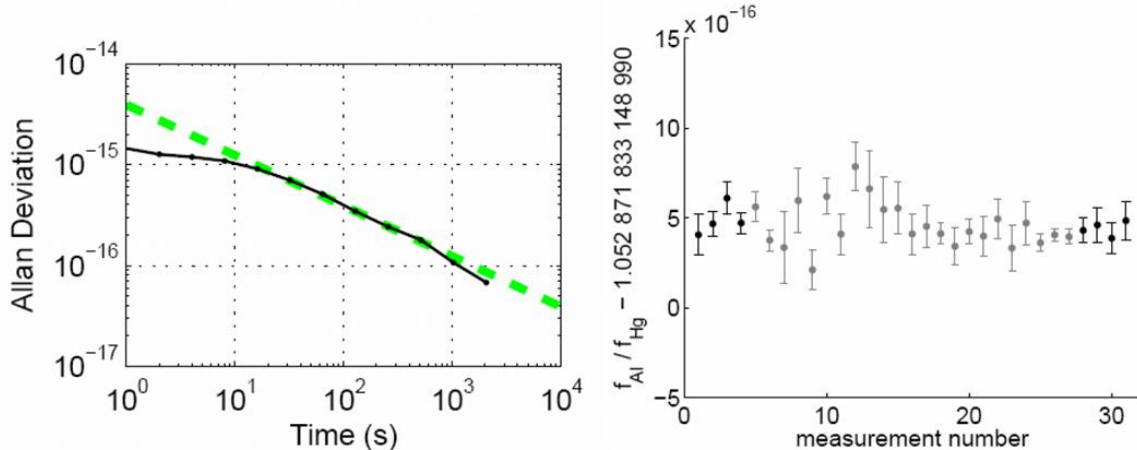


FIG. 1: a) Stability plot for the most recent Al^+/Hg^+ frequency ratio measurement. b) Historical record of the Al^+/Hg^+ measurements. Only the last four points have a comprehensive 1st order Doppler shift evaluation

the ratio is dominated by the statistical fractional frequency uncertainty of the measurement ($4.3 \cdot 10^{-17}$), leading to a total fractional frequency uncertainty of $5.2 \cdot 10^{-17}$. The statistical dispersion of the earlier data (first 27 points in figure 1b) with respect the last four data offers confidence in the reproducibility of the earlier measurements. Data corresponding to frequency ratio measurements made simultaneously by the two completely independent FSFCs were consistent to the order of the fractional frequency uncertainty of the ratio measurement made by either FSFC [27].

IV. TEST ON PHYSICAL THEORIES

A. Test on the temporal stability of α

The fine structure constant $\alpha = \frac{e^2}{4\pi\epsilon_0\hbar c}$ is the natural scaling factor for the energies involved in atomic spectroscopy including electronic, fine (FS) and hyperfine (HFS) structure. The energies or frequencies of each of these can be written as a function of a non-relativistic part, and a relativistic part $F_j(\alpha)$, which depends on the specific transition j that is considered. Following the theoretical treatment of Karshenboim, we write the transition frequencies in the following manner [28], [29]:

$$\begin{aligned} \nu_j(el) &= R_y F_j(\alpha) \\ \nu_j(FS) &= \alpha^2 R_y F_j(\alpha) \\ \nu_j(HFS) &= \alpha^2 \frac{\mu}{\mu_B} R_y F_j(\alpha) \end{aligned} \quad (2)$$

where R_y is the Rydberg constant, $\frac{\mu}{\mu_B}$ is the ratio between the magnetic moment of the nucleus μ and the Bohr magneton μ_B . Relative sensitivity of $\nu_j(el)$ and $\nu_j(HFS)$ with respect to a temporal variation of fundamental constants can be written by first taking the logarithm of these two terms and then differentiating with respect to time:

$$\begin{aligned} \frac{d \ln \nu_j(el)}{dt} &= \frac{d \ln R_y}{dt} + N_j \frac{d \ln \alpha}{dt} \\ \frac{d \ln \nu_j(HFS)}{dt} &= \frac{d \ln R_y}{dt} + \frac{d \ln(\mu/\mu_B)}{dt} \\ &\quad + (2 + N_j) \frac{d \ln \alpha}{dt} \end{aligned} \quad (3)$$

where $N_j \equiv \frac{d \ln F_j(\alpha)}{d \ln \alpha}$ contains the dependence of the specific transition involved. N_j can be either positive or negative, and tends to be larger for transitions involving heavier atoms, where relativistic corrections play a more important role. Values of N_j have been calculated for several electronic transitions of atomic and

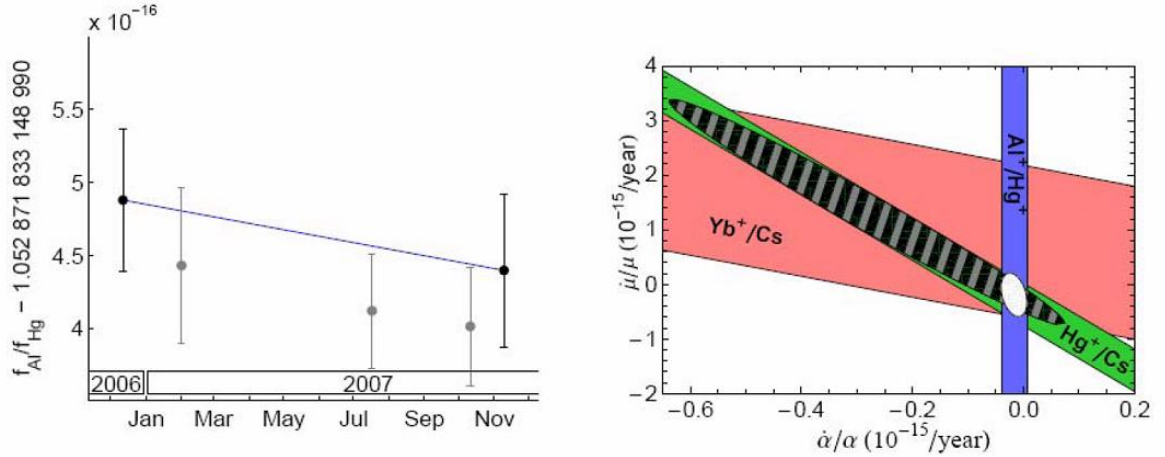


FIG. 2: a) Temporal variation of α is estimated with the line connecting the two extreme points, which are separated by a duration of a year b) Coupled constraint of $\dot{\alpha}/\alpha$ and $d/dt \ln(\mu_{Cs}/\mu_B)$. Projection of the the white ellipse on the x and y axes provides the results of equation 8 [20]

molecules of cosmological and laboratory interest, including Hg^+ [2] and Al^+ [30], as well as for HFS transitions involved in atomic frequency standards [2], [31].

From 3, the temporal sensitivity of the ratio between Hg^+ and Cs can be expressed as:

$$\frac{d}{dt} \left(\frac{\nu_{Hg^+}}{\nu_{Cs}} \right) = \frac{\dot{\alpha}}{\alpha} N - \frac{d}{dt} \ln \left(\frac{\mu_{Cs}}{\mu_B} \right) \quad (4)$$

where $N = N_{Hg^+} - N_{Cs} - 2$ and $N_{Hg^+} \approx -3.2$, $N_{Cs} \approx 0.8$. This gives a coupled constraint to any variations of α and $\left(\frac{\mu_{Cs}}{\mu_B} \right)$, for example, with time. By combining the results of frequency comparison experiments between different optical clocks and Cs, each offering different values for N , it is possible to constrain the variation of α and $\left(\frac{\mu_{Cs}}{\mu_B} \right)$ at the same time. This kind of analysis has been performed with a technique described in [32] and the results reported here come from [29]. The fractional uncertainty of the coupled variations can be estimated using a two-dimensional chi-square function for the 1σ statistical limit, and projecting the ellipse on the x and y axis gives the following temporal constraints:

$$\begin{aligned} -1.5 \cdot 10^{-15} < \frac{\dot{\alpha}}{\alpha} < 0.4 \cdot 10^{-15} \text{yr}^{-1} \\ -2.7 \cdot 10^{-15} < \frac{d}{dt} \ln \left(\frac{\mu_{Cs}}{\mu_B} \right) < 8.6 \cdot 10^{-15} \text{yr}^{-1} \end{aligned} \quad (5)$$

The measurement of the frequency ratio of Al^+ to Hg^+ provides a cleaner temporal constraint on $\dot{\alpha}/\alpha$ for several reasons. Firstly, the measurement is a direct comparison of the Al^+ and Hg^+ frequencies independent of their comparison to Cs. Hence it does not involve the Cs metric. Secondly, the transitions are both electronic to and to first order independent of any nuclear magnetic moments. The sensitivity on $\dot{\alpha}/\alpha$ given by the Al^+ to Hg^+ ratio is also high, owing to the large negative relativistic contribution for Hg^+ and the high accuracy of the measurement data. From equation 4 we can write:

$$\frac{d}{dt} \left(\frac{\nu_{Al^+}}{\nu_{Hg^+}} \right) = \frac{\dot{\alpha}}{\alpha} N \quad (6)$$

where $N = N_{Hg^+} - N_{Al^+} \approx -3.2$ and $N_{Al^+} \approx 0$. For the evaluation of $\dot{\alpha}/\alpha$, measurements data reported in figure 1b were con-

densed in five points, spanning from December 2006 to December 2007.

The line connecting the two extreme points provides the following constraint on the variation of the frequency ratio [20]:

$$\frac{d}{dt} \ln \left(\frac{\nu_{Al^+}}{\nu_{Hg^+}} \right) = (-5.3 \pm 7.9) \cdot 10^{-17} yr^{-1} \quad (7)$$

which is a ten-fold improvement to the best previous result. The intermediate points were excluded since the evaluation of their systematic uncertainties was incomplete. Based on this we can offer a more stringent limit on the temporal variation of α . Given the coupling between $\dot{\alpha}/\alpha$ and $d/dt \ln(\mu_{Cs}/\mu_B)$ in measurements between the Hg^+ clock and the Cs fountain, this also allows us to improve the constraint on variation of $d/dt \ln(\mu_{Cs}/\mu_B)$ using the data presented in [29]. As the

Al^+/Hg^+ frequency ratio does not depend on $d/dt \ln(\mu_{Cs}/\mu_B)$, it is represented as a vertical band in figure 2b. Projecting the white ellipse of figure 2b on the x and y axis the following updated estimation can be obtained:

$$\begin{aligned} \frac{\dot{\alpha}}{\alpha} &= (-1.6 \pm 2.3) \cdot 10^{-17} yr^{-1} \\ \frac{d}{dt} \ln \left(\frac{\mu_{Cs}}{\mu_B} \right) &= (-1.9 \pm 4.0) \cdot 10^{-16} yr^{-1} \end{aligned} \quad (8)$$

B. Acknowledgements

A. Bruschi recognizes financial support from the Danish Research Council. This work was partially supported by both the Office of Naval Research and NIST, agencies of the U. S. government; it is not subject to U. S. copyright.

-
- [1] T. Damour and F. Dyson, Nucl. Phys. B **480**, 37 (1996).
 - [2] V. A. Dzuba, V. V. Flambaum, and J. K. Webb, Phys. Rev. A **59**, 230 (1999).
 - [3] V. V. Flambaum, Int. J. Mod. Phys. A **22(27)**, 4937 (2007).
 - [4] S. Lea, Rep. Prog. Phys. **70**, 1773 (1995).
 - [5] W. H. Oskay, W. M. Itano, , and J. C. Bergquist, Phys. Rev. Lett. **94**, 163001 (4) (2006).
 - [6] T. Rosenband, P. O. Schmidt, D. B. Hume, W. M. Itano, T. M. Fortier, J. E. Stalnaker, K. Kim, S. A. Diddams, J. C. J. Koelemeij, J. C. Bergquist, et al., Phys. Rev. Lett. **98**, 220801 (2007).
 - [7] G. Wilpers, C. Oates, S. Diddams, A. Bartels, T. Fortier, W. Oskay, J. Bergquist, S. Jefferts, T. Heavner, T. Parker, et al., Metrologia **44**, 146 (2007).
 - [8] Z. Barber, C. Hoyt, C. Oates, L. Hollberg, A. Taichenachev, and V. Yudin, Phys. Rev. Lett. **96**, 083002 (4) (2006).
 - [9] S. R. Jefferts, J. H. Shirley, T. E. Parker, T. P. Heavner, D. M. Meekhof, C. W. Nelson, F. Levi, G. Costanzo, A. DeMarchi, R. E. Drullinger, et al., Metrologia **39**, 321 (2002).
 - [10] M. E. Poitzsch, J. C. Bergquist, W. M. Itano, and D. J. Wineland, Rev. Sci. Instrum. **67**, 129 (1996).
 - [11] D. J. Berkeland, F. C. Cruz, and J. C. Bergquist, Appl. Optics **36**, 4159 (1997).
 - [12] D. J. Berkeland and M. G. Boshier (2006), Private Communication.
 - [13] W. M. Itano, J. C. Bergquist, A. Bruschi, S. A. Diddams, T. M. Fortier, T. P. Heavner, L. Hollberg, D. B. Hume, S. R. Jefferts, L. Lorini, et al., in *Proc. 2007 SPIE Conf.* (2007), vol. 6673, p. 667303.
 - [14] L. L. et al., in *To be published in proceedings in EPJ Special Topics (????)*.
 - [15] R. W. P. Drever, J. L. Hall, and al., Appl. Phys. B **31**, 97 (1983).
 - [16] B. C. Young, F. C. Cruz, J. C. Bergquist, and W. M. Itano, Phys. Rev. Lett. **82**, 3799 (1999).
 - [17] J. Bergquist, W. Itano, and D. Wineland, in *Proc. 1992 Intl. School Phys. E.Fermi* (1992), pp. 359–376.
 - [18] H. Dehmelt, IEEE Trans. on Instr. and Meas. **IM-31**, 83 (1982).
 - [19] W. H. Oskay, S. A. Diddams, E. A. Donley, T. Fortier, T. P. Heavner, L. Hollberg, W. M. Itano, S. R. Jefferts, M. J. Jensen, K. Kim, et al., Phys. Rev. Lett. **97**, 020801(4) (2006).
 - [20] T. Rosenband, D. B. Hume, P. O. Schmidt, C. W. Chou, A. Bruschi, L. Lorini, W. H. Oskay, R. E. Drullinger, T. M. Fortier, J. E. Stalnaker., et al., Science **319** (**5871**), 1808 (2008).

- [21] D. J. Berkeland, J. D. Miller, J. C. Bergquist, W. M. Itano, and D. J. Wineland, *J. Appl. Phys.* **83**, 5025 (1998).
- [22] W. Itano, *J. Res. Natl. Inst. Stan.* **105**, 829 (2001).
- [23] M. Barrett, B. L. DeMarco, T. Schaetz, D. Leibfried, J. Britton, J. Chiaverini, W. M. Itano, B. M. Jelenkovic, J. D. Jost, C. Langer, et al., *Phys. Rev. A* **68**, 042302(7) (2003).
- [24] D. Wineland, J. Bergquist, J. Bollinger, R. Drullinger, and W. Itano, in *Proc. 2001 Freq. Stand. Metrology Symp.* (2001), pp. 361–368.
- [25] P. O. Schmidt, T. Rosenband, C. Langer, W. M. Itano, J. C. Bergquist, and D. J. Wineland, *Science* **309**, 749 (2005).
- [26] T. Rosenband, W. M. Itano, P. Schmidt, D. Hume, J. Koelemeij, J. C. Bergquist, and D. J. Wineland, in *Proc. 2006 EFTF Conf.* (2006), pp. 289–292.
- [27] I. Coddington, W. C. Swann, L. Lorini, J. C. Bergquist, Y. L. Coq, C. W. Oates, Q. Quraishi, K. S. Feder, J. W. Nicholson, P. S. Westbrook, et al., *Nature Photonics* **1**, 283 (2007).
- [28] S. G. Karshenboim, *Can. J. Phys.* **78**, 639 (2000).
- [29] T. Fortier, N. Ashby, J. C. Bergquist, M. J. Delaney, S. A. Diddams, T. P. Heavner, L. Hollberg, W. M. Itano, S. R. Jefferts, K. Kim, et al., *Phys. Rev. Lett.* **98**, 070801(4) (2007).
- [30] E. J. Angstrom, V. A. Dzuba, and V. V. Flambaum, *Phys. Rev. A* **70** **22(27)**, 014102 (2004).
- [31] H. Marion, F. P. D. Santos, M. Abgrall, S. Zhang, Y. Sortais, S. Bize, I. Maksimovic, D. Calonico, J. Gruenert, C. Mandache, et al., *Phys. Rev. Lett.* **90**, 150801 (2003).
- [32] E. Peik and al., *Phys. Rev. Lett.* **93**, 170801 (2004).